Full three-dimensional isotropic transformation media

C García-Meca[1,3], R Ortuño[2], J Martí[1] and A Martínez[1]

[1] Nanophotonics Technology Center, Universitat Politècnica de València, Valencia, 46022, Spain
[2] TERALAB (MmW–THz–IR & Plasmonics Laboratory), Universidad Pública de Navarra, Campus Arrosadía, Pamplona, 31006, Spain
E-mail: cargarm2@ntc.upv.es

Abstract

We present a method that enables the implementation of full three-dimensional (3D) transformation media with minimized anisotropy. It is based on a special kind of shape-preserving mapping and a subsequent optimization process. For sufficiently smooth transformations, the resulting anisotropy can be neglected, paving the way for practically realizable 3D devices. The method is independent of the considered wave phenomenon and can thus be applied to any field for which a transformational technique exists, such as acoustics or thermodynamics. Full 3D isotropy has an additional important implication for optical transformation media, as it eliminates the need for magnetic materials in many situations. To illustrate the potential of the method, we design 3D counterparts of transformation-based electromagnetic squeezers and bends.

Keywords: metamaterials, transformation optics, quasi-conformal mappings

1. Introduction

Transformation optics is currently becoming a mainstay in the design of photonic devices with advanced functionalities. Essentially, this technique provides a link between a coordinate transformation and the optical medium that would force light to follow the distortion encoded by such a transformation [1, 2]. Its use has enabled the achievement of unprecedented effects

---

[3] Author to whom any correspondence should be addressed.

such as invisibility and other optical illusions [3–7]. Inspired by transformation optics, the transformational paradigm has been gradually unfolding in other areas of physics, e.g., acoustics [8–12], elasticity [13], quantum mechanics [14] and thermodynamics [15]. However, the price to pay for the wave manipulation flexibility offered by this method is that general transformations are usually associated with complex media. Specifically, any distribution of inhomogeneous and anisotropic medium properties may arise from an arbitrary transformation. Even with the advent of metamaterials, it is extremely difficult to independently control all components of a certain tensorial property. For instance, constructing inhomogeneous devices with arbitrary anisotropic optical parameters that do not display undesired couplings between different polarizations is a challenging task. Similar couplings usually occur between pressure and shear waves in anisotropic elastic materials [16, 17].

In the case of optics, this fact is further complicated by the need for magnetic materials not available in nature, especially at high frequencies [18]. Although magnetic permeabilities can be artificially synthesized, their realization requires the use of resonant elements exhibiting a narrow-band response and, usually, high losses. If we restrict ourselves to two-dimensional (2D) transformations and propagation directions parallel to the transformation plane (say XY plane), a possible solution relies on limiting the device operation to one polarization. This way, a reduced set of feasible parameters produces the desired effect [3]. Another solution consists of using conformal mappings (CMs), which preserve the isotropy of the original space in the XY plane [1]. Although the resulting off-plane and in-plane parameters are different, it can be shown that isotropic non-magnetic materials provide exact implementations of CM for transverse electric waves (E-field along the *z*-direction) [7]. In the ray optics approximation, this is also valid for any polarization as long as the wave propagates parallel to the XY plane. When a CMs mapping the original region of interest to the desired one does not exist, we can resort to quasi-conformal mappings (QCMs), which restrict anisotropy to small negligible values [19, 20].

Unfortunately, in 3D the situation dramatically worsens. In this case, the implementation of the magnetic response associated with general anisotropic transformations cannot be avoided if the device is to work for any direction and polarization (this holds in the geometrical approximation). Even if the transformation is conformal in 2D, it cannot be implemented with all-dielectric parameters for off-plane propagation directions. The ideal solution would be to use 3D CMs giving rise to isotropic media, since the synthesis of highly anisotropic 3D materials is significantly more difficult than that of isotropic materials [16, 17]. Moreover, in the optical case we can omit the magnetic properties of isotropic materials without affecting the dynamics of rays.

However, the only existing CMs in 3D are Möbius transformations (similarities and inversions on spheres), which severely limits the range of implementable functionalities [21]. Certain approaches have been proposed to simplify the medium parameters associated with 3D transformations. In [16], 2D QCMs are mapped to 3D ones with revolution symmetry. Although the resulting parameters are still anisotropic, the device can be implemented with dielectric isotropic media for wave vectors with no azimuthal component. However, an additional magnetic component is necessary for other directions. In [18], it was shown that wave propagation in spherically symmetric anisotropic dielectric media can be independently engineered for each polarization, although with different functionalities. Finally, feasible realizations of different devices have been demonstrated for situations in which only propagation in specific directions is of interest [17, 22, 23]. Therefore, existing solutions still

impose strong restrictions, while the anisotropy requirement remains in the general 3D case, rendering the implementation of 3D transformation media technologically challenging.

Here, we develop a method that enables the implementation of full 3D transformations with small anisotropy. For sufficiently smooth transformations the anisotropy can be neglected, leading to isotropic media (and non-magnetic in the electromagnetic case). To illustrate its potential, we design 3D isotropic counterparts of two 2D electromagnetic transformational devices; namely, a squeezer and a bend [24–28]. Nonetheless, the method is independent of the considered wave phenomenon and can thus be applied to any other field for which a transformational technique exists, such as acoustics or thermodynamics.

2. Method

With the exception of Möbius transformations, CMs are found exclusively in 2D spaces. QCMs are sometimes thought of as existing only in 2D for this reason and, so far, they have been overlooked as a tool to achieve quasi-isotropic 3D transformation media. However, QCMs exist in any number of dimensions and form a much larger set than conformal ones [29]. This is because, while infinitesimal spheres preserve their spherical shape under a CM, QCMs transform spheres into ellipsoids of bounded eccentricity. The question is whether we can find 3D QCMs that introduce a degree of anisotropy sufficiently low so as to be negligible in practice. Here, we employ a recently-developed mapping technique based on Green coordinates (GCs) [30, 31] to give a positive answer. GCs use a cage-based representation in which each point within a simplicial surface (cage or mesh made up of triangles) is expressed as a linear combination of the cage vertices and faces normals

$$\boldsymbol{x} = \sum_{i \in I_{\mathbb{V}}} \phi_i(\boldsymbol{x}) \boldsymbol{v}_i + \sum_{j \in I_{\mathbb{T}}} \psi_j(\boldsymbol{x}) s_j \boldsymbol{n}_j, \tag{1}$$

where $\boldsymbol{v}_i$ is the ith vertex, $\boldsymbol{n}_j$ is the outward normal to the jth triangle, $s_j = 1$, and $I_{\mathbb{V}}$ and $I_{\mathbb{T}}$ are the sets of all vertices and triangles, respectively (see figure 1). A point $\boldsymbol{x}$ is univocally specified by the functions $\phi_i(\boldsymbol{x})$ and $\psi_j(\boldsymbol{x})$, known as GCs (the derivation of these functions is based on Green's third identity [30]). A certain transformation $\bar{\boldsymbol{x}} = f(\boldsymbol{x})$ is achieved just by deforming the cage; that is, (1) gives the transformed points $\bar{\boldsymbol{x}}$ if we replace $\boldsymbol{v}_i$ and $\boldsymbol{n}_j$ by the vertices $\bar{\boldsymbol{v}}_i$ and normals $\bar{\boldsymbol{n}}_j$ of the deformed cage. This way, the change $\boldsymbol{v}_i \to \bar{\boldsymbol{v}}_i$ defines a mapping f for all points enclosed by the cage. The most interesting property of GC transformations is that they are least distorting (i.e., they minimize anisotropy) when the scalars s_j are also a proper function of the jth triangle vectors [30] (see appendix). Thus, they are good candidates to attain quasi-isotropic transformation media. One just needs to enclose the region to be transformed by a cage and deform it as desired. All points inside the cage will follow this transformation in a low-distorting way. An additional advantage of GCs is that they are based on closed analytical expressions, so no meshing or numerical approximations are required [30]. Moreover, any transformation can be simply calculated as a linear combination of the precalculated coordinates as shown by equation (1).

However, although GC transformations provide 3D QCMs, we found that in most cases the resulting anisotropy is not low enough to be negligible. To overcome this drawback, we exploit the fact that a certain functionality can be implemented by a wide range of transformations and seek the one that is closest to a conformal one through optimization. In
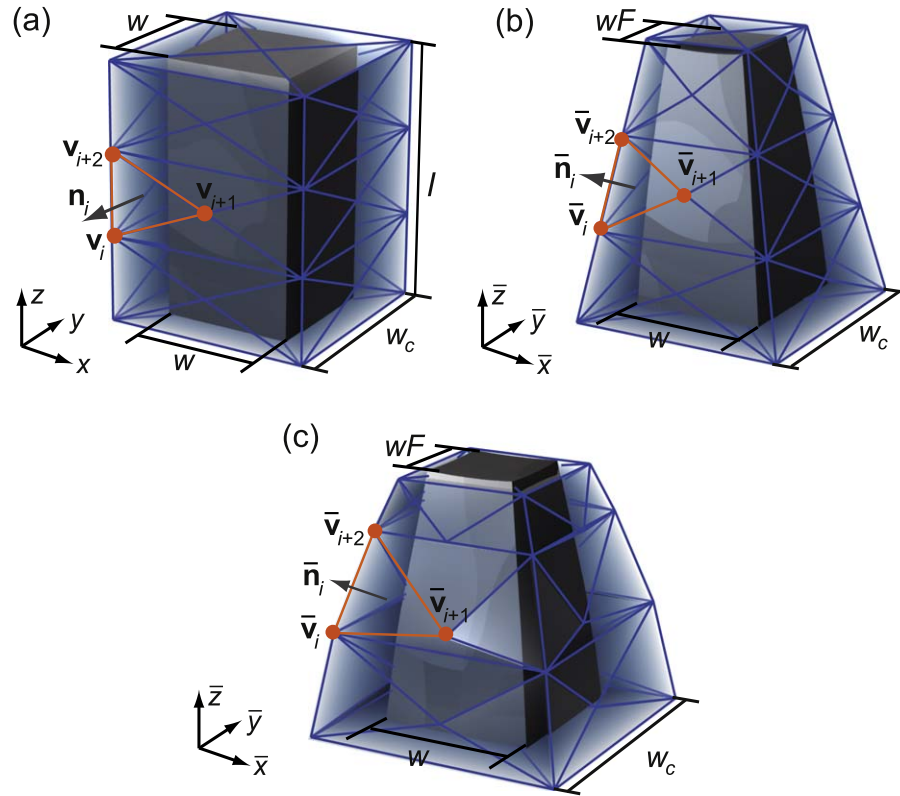
Figure 1. Green coordinate transformations. (a) The region to be transformed (gray square prism in this case) is enclosed by a cage made up of triangles. A cage deformation ($v_i \rightarrow \bar{v}_i$) defines a smooth mapping for all prism points, which follows the cage deformation in a low-distorting way. (b) Result of a transformation in which the cage is linearly compressed. (c) Optimized cage that minimizes anisotropy and corresponding transformed prism.

order to measure the degree of anisotropy introduced by a certain 3D transformation, we define in analogy with the 2D case an anisotropy factor $\alpha = \max_{\forall x}\{n_1/n_2, n_1/n_3, n_2/n_3\}$, which starts at 1 (no anisotropy) and grows with the anisotropy. Here, n_i are the principal components of the refractive index tensor in a local Cartesian system ($n_1 > n_2 > n_3$). The refractive index tensor can be obtained from the permittivity $\epsilon^{\bar{i}\bar{j}}$ and permeability $\mu^{\bar{i}\bar{j}}$ associated with a certain transformation, which are given by $\epsilon^{\bar{i}\bar{j}} = \mu^{\bar{i}\bar{j}} = \Lambda_i^{\bar{i}}\Lambda_j^{\bar{j}}\delta^{ij}/\det(\Lambda_i^{\bar{i}})$, where $\Lambda_i^{\bar{i}}$ is the transformation Jacobian matrix (we assume that the original medium is a vacuum) [2, 7].

3. Examples

In this section, we use the proposed method to design 3D isotropic counterparts of two well-known 2D electromagnetic transformational devices; namely, a squeezer and a bend. Transformation-based squeezers have been extensively studied due to their simplicity and potential applications. Isotropic 2D squeezers can be easily achieved by using standard QCM algorithms [27, 28]. Unfortunately, existing 3D designs are highly anisotropic. For instance, imagine that we want to gradually compress the gray square prism shown in figure 1, from zero
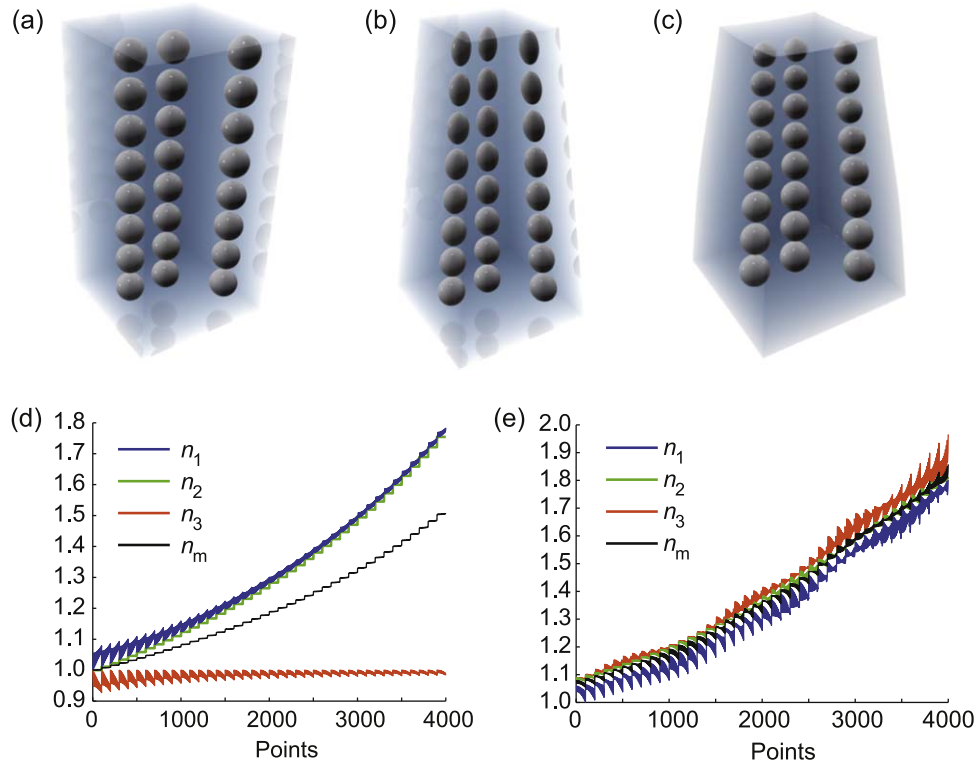
Figure 2. 3D squeezing transformations. (a) Original prism and some spherical regions within it. (b), (c) Prism and sphere transformations associated with a linear mapping and the proposed 3D QCM, which preserves spherical shapes. (d), (e) Refractive index corresponding to the linear and 3D QCM.

compression at $z = 0$ to a compression factor F at $z = l$ (the results are independent of the length scale so we work in arbitrary units). If we employ a linear transformation such as $\bar{x} = x(1 + az)$; $\bar{y} = y(1 + az)$; $\bar{z} = z$, with $a = (F - 1)/l$, a strong anisotropy is introduced. As an example, for $F = 0.57$ (reduction of the output face to one-third of its initial area), $l = 2$ and $w = 1$ we obtain $\alpha = 1.81$. The corresponding values of n_i in a 3D grid covering the whole transformed volume are shown in figure 2(d). Clearly, there is a marked discrepancy between the different components. A nice way to visualize the degree of anisotropy is to see how some small spheres within the original prism are transformed (figure 2(a)). As seen, the spherical shape is not preserved when using the previous linear transformation (figure 2(b)). Now we apply the proposed method. To do so, we surround the prism by a cage consisting of 30 vertices and 56 triangles (figure 1(a)). Note that the cage has a width $w_c = 1.6$, larger than w. The reason is that we found that a high distortion usually appears near the cage boundaries. Initially, we transformed the vertices using the above-mentioned linear mapping. GCs are not interpolatory and it is not guaranteed that compressing the cage by a certain factor will yield a prism compression of the same factor. Actually, in this case the side of the cage output face must be compressed by a factor around 0.5 to achieve the desired value of 0.57. This GC transformation automatically reduces anisotropy to $\alpha = 1.31$. However, this is not a value low enough to be negligible. Fortunately, we can use the fact that we are only interested in having a compressed version of the field at the squeezer output, and we do not care about how the fields are transformed inside the squeezer. Thus, the only restrictions are that the shape of the input
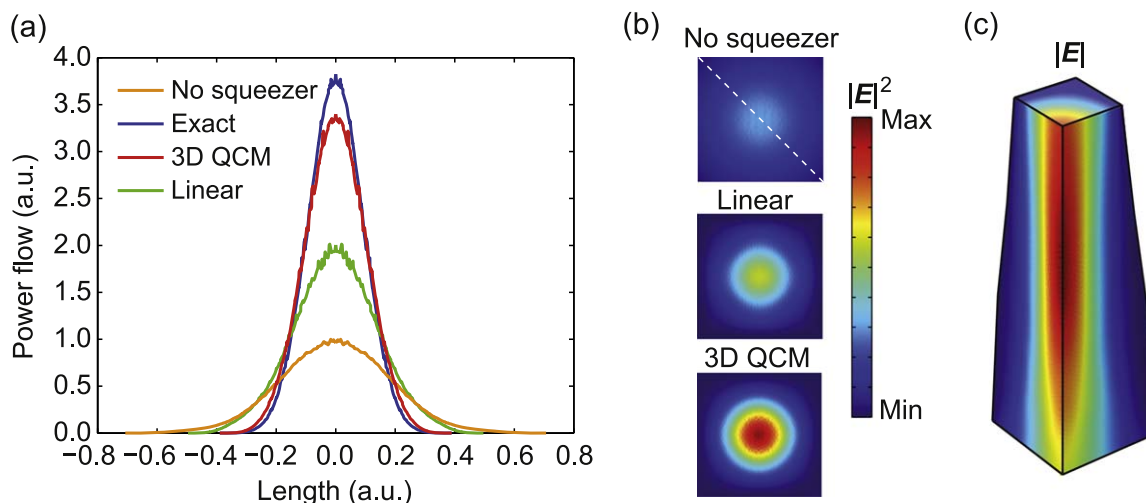
Figure 3. Squeezer performance. (a) Power flow in the propagation direction along a diagonal (dashed line in (b)) of the output face for the different squeezer versions and power flow of the beam after propagating a distance l in free space. (b) $|\boldsymbol{E}|^2$ distributions at the output face. (c) Beam $|\boldsymbol{E}|$-field cuts in its propagation through the GC isotropic squeezer. The wavelength is taken to be 0.15.

surface should not be changed by the transformation and that the transformed output surface must be a compressed version of the original one. Hence, the position of all the vertices that do not belong to these faces, as well as the squeezer height, can be optimized to minimize anisotropy. This is done through a standard Nelder–Mead algorithm [32]. It is worth mentioning that another advantage of GCs is that optimizing a transformation only requires the tuning of a few variables (vertex positions), which completely define the mapping. Taking advantage of the symmetries, we only need to optimize 11 variables to obtain a suitable transformation of the prism (see figure 1(c)). The corresponding index eigenvalues are shown in figure 2(e). They are remarkably close to each other, indicating a low anisotropy. This confirms the fact that this mapping hardly distorts the shape of small spheres (figure 2(c)). In fact, a very low anisotropy factor of 1.08 is obtained after optimization. This is of the order of the values obtained in 2D QCMs [19] and allows us to neglect the anisotropy. We do this by approximating the anisotropic index by an isotropic one n_{m} equal to the mean of its principal components $n_{\mathrm{m}} = (n_1 + n_2 + n_3)/3$ i.e., we take $\epsilon^{\bar{\imath}\bar{\jmath}} = \mu^{\bar{\imath}\bar{\jmath}} = n_{\mathrm{m}}\delta^{\bar{\imath}\bar{\jmath}}$.

To verify its functionality, the designed 3D squeezer is simulated in COMSOL Multiphysics. A Gaussian beam is used as the source. Figure 3(a) shows the power flow in the propagation direction along a diagonal of the output face for different cases. The power at the output of the exact anisotropic squeezer (blue) is a perfect compressed version of the beam power flow after propagating a distance l in free space (orange). Very similar results are obtained for the isotropic GC-based squeezer, confirming that neglecting the anisotropy hardly affects the squeezer performance. Moreover, almost the same results are obtained by dropping the magnetic permeability; i.e., taking $\epsilon^{\bar{\imath}\bar{\jmath}} = n_{\mathrm{m}}^2\delta^{\bar{\imath}\bar{\jmath}}$ and $\mu^{\bar{\imath}\bar{\jmath}} = \delta^{\bar{\imath}\bar{\jmath}}$ (red). However, if we approximate the index of the linear-transformed squeezer by the mean of its eigenvalues, its performance is significantly deteriorated (green). The field profiles at the output face for the free-space case and the GC and linear isotropic squeezers are shown in figure 3(b). Different
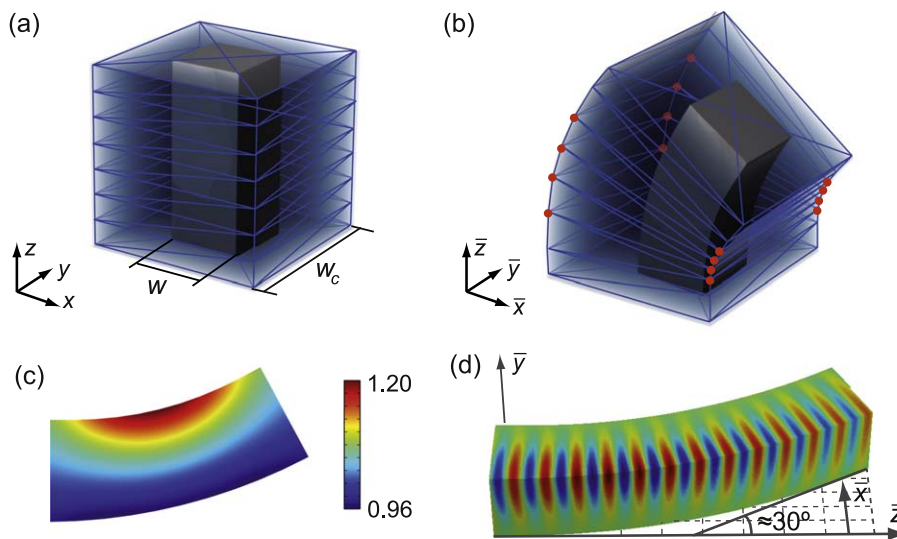
Figure 4. 3D bend. (a) Original prism and enclosing cage ($w = 0.8$, $w_c = 2$). (b) Deformed cage and transformed prism. (c) Final bend refractive index in the plane $y = 0$. (d) Propagation of a Gaussian beam throughout the 3D bend.

cuts of the |**E**|-field along its propagation through the GC isotropic squeezer are depicted in figure 3(c).

Finally, although the functionality of the GC-based squeezer is almost the desired one, it is worth trying to explain the slight worsening resulting from replacing the exact index by its mean value. It is known that a 3D isotropic refractive index n_m can be interpreted as the implementation of a metric given by $g_{ij} = n_m^2 \delta_{ij}$. Starting from an empty virtual space, this metric can only be the result of either a Möbius coordinate transformation or of virtual space being curved [7]. Therefore, the average of the slightly anisotropic index associated with a GC-based QCM no longer represents the initial transformation and will generally correspond to a curved virtual space or, exceptionally, to a different transformation. This will result in a small deviation from the desired functionality. Determining the exact origin (curved geometry or transformation) of this effective metric is very difficult and thus it is also difficult to predict what the specific mentioned deviation will be by any means other than a simulation. Nevertheless, as in the previous example, this effect will not usually be important thanks to the small anisotropy.

As a second example, we employ the proposed method to construct a 3D bend. We start from a square prism surrounded by a cage consisting of 34 vertices and 64 triangles (see figure 4(a)). Our goal is to bend the prism by 30° around the y-axis. To this end, we initially use the transformed cage shown in figure 4(b), where the orange vertices are optimized to minimize anisotropy. Considering the symmetries, this implies optimizing 12 variables. After the whole process, a value of $\alpha = 1.07$ is obtained. The refractive index of the device with neglected anisotropy in the plane $y = 0$ is rendered in figure 4(c). The propagation of a Gaussian beam along two orthogonal surfaces passing through the bend axis is depicted in figure 4(d). The beam is bent by approximately 30°, verifying the correct performance of the designed device. It is worth mentioning that, although the bending effect lies in planes orthogonal to the y-direction, the transformation is 3D, which allows us to attain a quasi-isotropic medium. This is different from existing bends based on 2D transformations, which are inherently anisotropic and
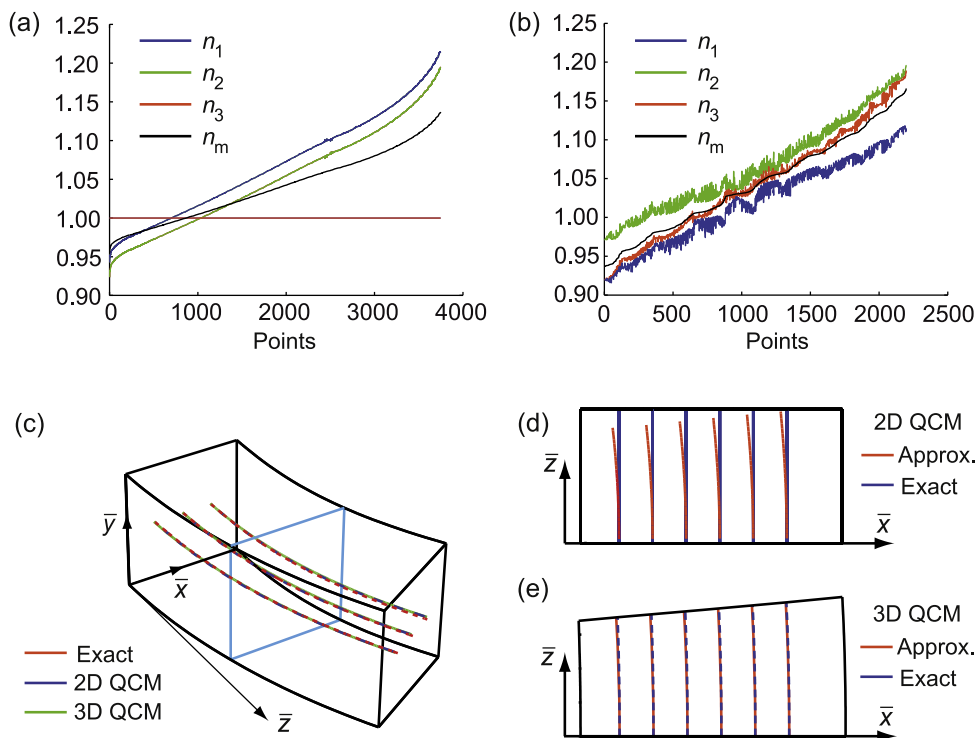
Figure 5. Comparison between different bends. (a) Principal components of the refractive index associated with a 2D QCM and (b) the proposed 3D QCM. (c) Rays propagating along the plane of the transformation for the considered 2D and 3D QCM with neglected anisotropy. Results are compared with the exact implementation of these transformations, which coincide in this case. (d), (e) Same as in (c) but for rays propagating in an XY plane (outlined in light blue in (c)).

require magnetic materials for a complete implementation. However, the effect of dropping the magnetic properties in the QCM-based bend designed here hardly alters its functionality. Naturally, it would be possible to bend the beam following any 3D curve, although this would require the optimization of a larger number of variables and computationally-intensive simulations (symmetries could not be exploited) exceeding our capabilities.

To complete the study, we compare the performance of the proposed bend with a similar device designed with another technique. Since the bending effect is 2D, the best option available is a 2D QCM. Hence, using a standard algorithm [20] we designed a bend with a shape very similar to that of the GC-based one. The principal components of the refractive index associated with each transformation are shown in figure 5. In the 2D QCM case, the in-plane components are very similar, but significantly different from the off-plane one, while in the 3D QCM case, all components are close to each other. Although the 2D anisotropy factor (which considers only the in-plane components) of the 2D QCM is very low ($\alpha = 1.02$), its 3D factor is 1.22. To compare both devices in a simple way, we analyze the trajectories followed by different rays by numerically solving Hamilton's equations [7]. We found that approximating the index components of the 2D QCM bend by its mean value completely destroys its expected behavior and thus, as usual, we approximate it by the mean of the in-plane components (the GC-based bend index is approximated by n_m as before). Regarding the propagation of rays along this plane, as expected, the performance of both devices is very similar, and very close to

the ideal trajectories determined by the exact implementation of both transformations (see figure 5(c)). The reason behind the good behavior of the 2D QCM bend is that only the in-plane index components intervene here. However, for other propagation directions the performance of the 2D QCM should deteriorate. To confirm this, although the bend was not devised to work for off-plane propagation, we launch several rays within both devices from the $\bar{y} = 0$ plane and directed towards the $\bar{y}$-direction (after neglecting anisotropy as described above) and compare the obtained trajectories with those associated with the corresponding exact implementations (without neglecting anisotropy). Figures 5(d) and (e) show the trajectories followed in each case until the instant at which the rays should reach the bend boundary (depicted in black). In the 2D QCM case, the simulated rays deviate significantly from their ideal trajectories and do not reach the boundary at the expected time. In the 3D case, simulated and ideal trajectories are very similar. Note that the faces of constant y in virtual space are not transformed to faces of constant $\bar{y}$ by the 3D QCM (we allowed this flexibility during the optimization process, something that cannot be done with a 2D transformation).

4. Conclusion

In conclusion, we have shown that the combination of 3D GC transformations and a suitable optimization process leads to a significant reduction of the typical anisotropy associated with 3D transformation media. In the case of sufficiently smooth transformations the anisotropy can be minimized to negligible values. The method is valid for any transformational technique, such as the ones developed for acoustics or thermodynamics. For instance, the studied transformations can be directly used to construct acoustic squeezers or bends by using mass density and bulk modulus distributions given by $\rho^{\bar{i}\bar{j}} = \Lambda_i^{\bar{i}} \Lambda_j^{\bar{j}} \rho^{ij}/\det(\Lambda_i^{\bar{i}})$ and $\bar{\kappa} = \det(\Lambda_i^{\bar{i}})\kappa$, respectively, where ρ^{ij} and κ are the parameters in virtual space. As in the electromagnetic case, the inverse mass density tensor $\rho^{\bar{i}\bar{j}}$ will display only a slight negligible anisotropy. Moreover, full 3D isotropy has an important implication for electromagnetic transformation media, whose magnetic properties can be dropped without affecting the dynamics of rays. Note that the proposed method only allows us to work with simply connected domains. Therefore, it is not suitable for designing invisibility cloaks based on opening holes in space. On the other hand, it could in principle be used to design less demanding cloaking devices, such as the so-called carpet cloak [19]. In addition, it is worth mentioning that the anisotropy arising from abrupt transformations might not be negligible. In those situations, and depending on the specific transformation, other kinds of mappings not based on GC [33], as well as more advanced optimization algorithms, could provide even better results. In any case, we can conclude that the use of special 3D QCM techniques could become a key enabling methodology to achieve practically realizable 3D transformation media.

Appendix A. Calculation of Green coordinates and associated transformations

The Green coordinates and associated transformations used in the examples analyzed in this work were calculated with MATLAB. The coordinate functions $\phi_i(x)$ and $\psi_j(x)$ are given by the following surface integrals

$$\phi_i(x) = -\iint_{r \in N(v_i)} \Gamma_i(r) \frac{\partial G(r, x)}{\partial n(r)} dS, \tag{A.1}$$

$$\psi_j(x) = -\iint_{r \in S_j} G(r, x) \, dS, \tag{A.2}$$

where S_j is the surface of the jth triangle (referred to as t_j from now on), $n(r)$ is the normal to the triangle on which r lies, $N(v_i)$ is the union of all faces in the one-ring neighborhood of v_i, and $\Gamma_i(r)$ is the piecewise linear hat function defined on $N(v_i)$ that is one at v_i and zero at all other vertices. In 3D, $G(r, x)$ is the Green's function

$$G(r, x) = \frac{-1}{4\pi |r - x|}, \tag{A.3}$$

and the scaling factors s_j required for the calculation of least-distorting transformations are

$$s_j = \frac{\left[|\bar{u}_j|^2 |w_j|^2 + |\bar{w}_j|^2 |u_j|^2 - 2\left(\bar{u}_j \cdot \bar{w}_j\right)(u_j \cdot w_j) \right]^{1/2}}{\sqrt{8} \, S_j}, \tag{A.4}$$

where u_j and w_j are the vector edges that define the initial jth triangle (see figure A1(a)), and $\bar{u}_j$ and $\bar{w}_j$ their transformed counterparts. Note that A.1 and A.2 can be expressed in closed analytical form [30, 31]. Next, we include a summary of the results required for the analytical calculation of GC in 3D.

First, to calculate the integral in A.2, we divide each triangle t_j into three smaller triangles Δ_i ($i = 1, 2, 3$) using the projection p of the point x over the plane where t_j lies (see figure A1(a)). Naming the vertices of this triangle as v_1^j, v_2^j and v_3^j, it can be shown that this integral can be expressed as

$$\psi_j(x) = \frac{1}{4\pi} \sum_{i=1}^{3} \text{sign}(\Delta_i) \left[\int_{\varphi = \delta_i - \beta_i}^{\delta_i} \left(c + \frac{\lambda_i}{\sin^2 \varphi} \right) d\varphi - \sqrt{c}\,\beta_i \right], \tag{A.5}$$

where

$$\lambda_i = |v_i^j - p|^2 \sin^2(\alpha_i), \tag{A.6}$$

$$\alpha_i = \text{acos}\left[\frac{(v_{i+1}^j - v_i^j) \cdot (p - v_i^j)}{|v_{i+1}^j - v_i^j| \; |p - v_i^j|} \right], \tag{A.7}$$

$$\beta_i = \text{acos}\left[\frac{\left(v_i^j - p\right) \cdot \left(v_{i+1}^j - p\right)}{\left|\left(v_i^j - p\right)\right| \; \left|v_{i+1}^j - p)\right|} \right], \tag{A.8}$$
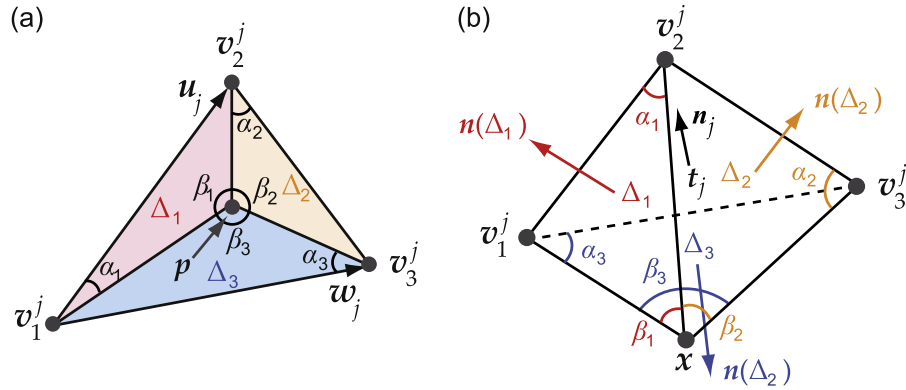
Figure A1. Calculation of Green coordinates. (a) Triangles involved in the calculation of $\psi(x)$. Here, $\Delta_1 = pv_1^j v_2^j$, $\Delta_2 = pv_2^j v_3^j$, and $\Delta_3 = pv_3^j v_1^j$. The vectors u_j and w_j, defined as $u_j = v_2^j - v_1^j$ and $w_j = v_3^j - v_1^j$, are also shown. (b) Triangles involved in the calculation of $\phi(x)$. In this case, $\Delta_1 = xv_2^j v_1^j$, $\Delta_2 = xv_3^j v_2^j$, and $\Delta_3 = xv_1^j v_3^j$.

$$c = |x - p|^2, \tag{A.9}$$

$$\delta_i = \pi - \alpha_i, \tag{A.10}$$

$$\text{sign}(\Delta_i) = \text{sign}\left\{ n_j \cdot \left[(v_i^j - p) \times (v_{i+1}^j - p) \right] \right\}, \tag{A.11}$$

with $i = 1, 2, 3$ and $v_4^j = v_1^j$. Note that all triangle normals should point outside the simplicial surface. Here, we named the vertices of triangle t_j in such a way that its normal is given by $n_j = (u_j \times w_j)/|u_j \times w_j|$.

Second, to obtain $\phi_i(x)$ we only need to know how to calculate the following surface integral over any given triangle t_j

$$\iint_{r \in S_j} \Gamma_i(r) \frac{\partial G(r, x)}{\partial n(r)} dS, \tag{A.12}$$

since $N(v_i)$ is the union of all triangles in the one-ring neighborhood of v_i. This integral is simplified if we set x as the origin of coordinates (note that GCs are independent of the choice of the coordinate origin) and consider the tetrahedron whose vertices are x and those of t_j (see figure A1(b)). In this case we arrive at the following identity

$$\iint_{r \in S_j} \Gamma_k^j(r) \frac{\partial G(r, x)}{\partial n(r)} dS = \frac{n(\Delta_{k+1}) \cdot \iint_{r \in S_j} r \frac{\partial G(r, x)}{\partial n(r)} dS}{n(\Delta_{k+1}) \cdot v_k^j}, \tag{A.13}$$

with $k = 1, 2, 3$ and where Γ_1^j, Γ_2^j and Γ_3^j are the hat functions associated with v_1^j, v_2^j and v_3^j, respectively. Here, $n(\Delta_k)$ denotes the normal to triangle Δ_k, with $\Delta_4 = \Delta_1$ (see figure A1(b) for a definition of these triangles). In addition, the integral on the right-hand side of A.13 can be expressed as

$$\iint_{r \in S_j} r \frac{\partial G(r, x)}{\partial n(r)} dS = -n_j \psi_j(x) - \frac{1}{4\pi} \sum_{i=1}^{3} n(\Delta_i) \int_{\varphi = \delta_i - \beta_i}^{\delta_i} \left(\frac{\lambda_i}{\sin^2 \varphi} \right) d\varphi, \quad (A.14)$$

with

$$\lambda_i = |v_{i+1}^j|^2 \sin^2(\alpha_i), \tag{A.15}$$

$$\alpha_i = \mathrm{acos} \left[\frac{(v_{i+1}^j - v_i^j) \cdot v_{i+1}^j}{|v_{i+1}^j - v_i^j| \; |v_{i+1}^j|} \right], \tag{A.16}$$

$$\beta_i = \mathrm{acos} \left[\frac{v_i^j \cdot v_{i+1}^j}{|v_i^j| \; |v_{i+1}^j|} \right], \tag{A.17}$$

$$\delta_i = \pi - \alpha_i. \tag{A.18}$$

Finally, the integrals appearing in A.5 and A.14 can be calculated using the following antiderivative

$$\int \sqrt{c + \frac{a}{\sin^2 \varphi}} \, d\varphi = \frac{-\mathrm{sign}(\sin \varphi)}{2} \left\{ 2\sqrt{c} \; \mathrm{atan} \left(\frac{\sqrt{c} \; \cos \; \varphi}{\sqrt{a + c \sin^2 \varphi}} \right) \right.$$

$$\left. + \sqrt{a} \; \ln \left[\frac{2\sqrt{a} \sin^2 \varphi}{(1 - \cos \; \varphi)^2} \left(1 - \frac{2c \; \cos \; \varphi}{c(1 + \cos \; \varphi) + a + \sqrt{a^2 + ac \sin^2 \varphi}} \right) \right] \right\}. \tag{A.19}$$

References

[1] Leonhardt U 2006 *Science* **312** 1777
[2] Pendry J B, Schurig D and Smith D R 2006 *Science* **312** 1780
[3] Schurig D, Mock J J, Justice B J, Cummer S A, Pendry J B, Starr A F and Smith D R 2006 *Science* **314** 977–80
[4] Greenleaf A, Kurylev Y, Lassas M and Uhlmann G 2007 *Phys. Rev. Lett.* **99** 183901
[5] Shalaev V M 2008 *Science* **322** 384
[6] Chen H, Chan C T and Sheng P 2010 *Nature Mater.* **9** 387
[7] Leonhardt U and Philbin T 2010 *Geometry and Light. The Science of Invisibility* (Mineola, NY: Dover Publications)
[8] Cummer S A and Schurig D 2007 *New J. Phys.* **9** 45
[9] Chen H and Chan C T 2007 *Appl. Phys. Lett.* **91** 183518
[10] Norris A N 2009 *J. Acoust. Soc. Am.* **125** 839
[11] Chen H and Chan C T 2010 *J. Phys. D: Appl. Phys.* **43** 113001
[12] García-Meca C, Carloni S, Barceló C, Jannes G, Sánchez-Dehesa J and Martínez A 2013 *Sci. Rep.* **3** 2009
[13] Norris A N and Shuvalov A L 2011 *Wave Motion* **48** 525
[14] Zhang S, Genov D A, Sun C and Zhang X 2008 *Phys. Rev. Lett.* **100** 123002
[15] Guenneau S, Amra C and Veynante D 2012 *Opt. Express* **20** 8207
[16] Landy N I, Kundtz N and Smith D R 2010 *Phys. Rev. Lett.* **105** 193902
[17] Urzhumov Y, Landy N and Smith D R 2012 *J. Appl. Phys.* **111** 053105

[18] Danner A J, Tyc T and Leonhardt U 2011 *Nature Photon.* **5** 357
[19] Li J and Pendry J B 2008 *Phys. Rev. Lett.* **101** 203901
[20] Chang Z, Zhou X, Hu J and Hu G 2010 *Opt. Express* **18** 6089–96
[21] Blair D E 2000 *Inversion Theory and Conformal Mapping* (Providence, RI: American Mathematical Society)
[22] Chen H and Zheng B 2012 *Sci. Rep.* **2** 255
[23] Landy N and Smith D R 2013 *Nature Mater.* **12** 25
[24] Rahm M, Schurig D, Roberts D A, Cummer S A, Smith D R and Pendry J B 2008 *Photon. Nanostruct. Fundam. Appl.* **6** 87
[25] Rahm M, Roberts D A, Pendry J B and Smith D R 2008 *Opt. Express* **16** 11555–67
[26] Schmiele M, Varma V S, Rockstuhl C and Lederer F 2010 *Phys. Rev. A* **81** 033837
[27] García-Meca C, Tung M M, Galán J V, Ortuno R, Rodríguez-Fortuno F J, Martí J and Martínez A 2011 *Opt. Express* **19** 3562
[28] Liu D, Gabrielli L H, Lipson M and Johnson S G 2013 *Opt. Express* **21** 14223
[29] Heinonen J 2006 *Not. Amer. Math. Soc.* **53** 1334
[30] Lipman Y, Levin D and Cohen-Or D 2008 *ACM Trans. Graph.* **27** 78
[31] Lipman Y and Levin D 2010 *Comput. Methods Funct. Theory* **10** 167–88
[32] Nelder J A and Mead R 1965 *Comput. J.* **7** 308
[33] Paillé G P and Poulin P 2012 *Comput. Graph.* **36** 427–33